Journal of Thermal Analysis and Calorimetry, Vol. 80 (2005) 103–108

KINETICS OF OXIDATION IN VARIOUS FORMS OF CARBON

Emília Illeková[1*] *and Katarína Csomorová*[2]

[1]Institute of Physics, Slovak Academy of Sciences, Dúbravská cesta 9, 845 11 Bratislava, Slovakia
[2]Polymer Institute, Slovak Academy of Sciences, Dúbravská cesta 9, 842 36 Bratislava, Slovakia

In this work the kinetics of the high-temperature oxidation of the powder amorphous carbon and bulk single-wall carbon nanotubes is studied. The thermal degradation of the sample is measured by differential scanning calorimetry using the continuous heating regime up to 1273 K. Also, the oxidation resistance of the samples is evaluated by the mass loss in a thermogravimetric analyzer. Both flowing and static oxygen and dry-air atmospheres are used. The specific role of the external diffusivity of the reagent gas is analyzed. The kinetics of the chemical reaction is specified using the Kissinger, Coats and Redfern methods.

Keywords: *amorphous carbon, DSC, kinetics, oxidation, SWCNT, TG*

Introduction

Elemental carbon can form a variety of structures. Apart from the well-known diamond and graphite (G), carbon can build concave cages with honeycomb atomic arrangement as e.g. closed fullerenes (C_{60}) or tubular structures as nanotubes. Also, considerable attention has been devoted to numerous amorphous carbon forms. Nowadays, along with the improvement of the techniques for the production of synthesized bulk samples, progress is being made in their experimental characterization and applications. The interaction of each bulk carbon form with the environment, especially the ability to react with the gases may significantly influence its thermodynamic stability and consequently its promising application properties. Most frequently, the hydrogen adsorption on carbon nanofibers is being investigated as for example in [1]. Illeková *et al*. [2] characterized the kinetics of desorption of the water vapor at temperatures above 260 K in various forms of the bulk carbon. Here, we report the interaction of molecular oxygen with amorphous carbon (AC) compared to that with the single-wall carbon nanotubes (SWCNT).

Experimental

The sample of commercial AC (Printex, powder, particle size <1 mm) consisted of few particles. That one of commercial purified single-wall carbon nanotubes (SWCNT) (CNI Texas, HiPco, ~3.5 mass% of Fe-containing catalyst, granular material, grain size ~1.3 mm) consisted always of one grain. Also the commercial polycrystalline graphite (G) (Merck, massive compressed pellet sample) was considered. Samples were stored in open-air atmosphere.

Calorimetric signals from phase transformations were monitored by differential thermal analyzer (DTA) using PerkinElmer DTA7 (the overall uncertainty of ±2 K; ±4 J g^{-1}) and DSC using PerkinElmer DSC7 (±0.5 K; ±2 J g^{-1}) systems. Continuous-heating regimes from 258 to 873 K for DSC and from 300 to 1273 K for DTA with heating rates, (β), ranging from 5 to 80 K min^{-1} were used. Samples of 0.01–0.37 mg, open wide and shallow Al pans, the flowing atmosphere (technical oxygen, 90 mL min^{-1}) for DSC and samples of 3.7–4.8 mg, both open and closed massive narrow and deep Al_2O_3 pans in both static and dynamic atmospheres (dry air, from 0 to 90 mL min^{-1}) for DTA were utilized. The empty pan was always used as a reference.

The thermogravimetric analyses (TG) were performed on the apparatus Mettler-Toledo TGA/SDTA 851^e (±0.5 K; ±2 μg) under the same experimental conditions: open Al_2O_3 crucibles, β from 2 to 40 K min^{-1}, dynamic atmosphere (technical oxygen, 80 mL min^{-1}), and sample mass of 0.102–0.140 mg.

DTA, DSC and TG instruments were calibrated for all heating rates using In, Zn, Al and Au standards.

The thermodynamic parameters were calculated using Pyris Software, Version 3.0. The subtracted 1st measuring run and the subsequently following 2nd run was always used for the kinetic calculations in the DSC and DTA experiments. (The 2nd run was taken as a baseline, being a blank in the case of AC and G samples.) Only the 1st measuring run was used in the TG experiments. Also the derivatives (DTG) of the original TG curves (and smoothed up to 100 points in the case of higher β) were computed.

* Author for correspondence: fyziille@savba.sk

1388–6150/$20.00

Akadémiai Kiadó, Budapest, Hungary
Springer, Dordrecht, The Netherlands

Results

The oxidation under nonisothermal conditions of fine-grained carbonaceous materials proceeds in several distinct temperature intervals. Figure 1 shows the DTA traces for AC and SWCNT compared to that of G in the flowing dry-air atmosphere and semi-closed sample pans. In the case of AC, the caloric effect of –28,980 J g^{-1} shows one sharp exothermal peak starting at $T_{x,AC}$=686 K (being the peak onset temperature), while in the case of SWCNT, two successive oxidation effects of –27,090 J g^{-1} starting already at $T_{x,SWCNT}$=625 K are significantly prolonged to temperatures above 1070 K. The total oxidation of G (–20,895 J g^{-1}), being the thermodynamically most stable modification of carbon, takes place at high temperatures starting at $T_{x,G}$=914 K. The thermal degradation (as will be shown later) evidenced that the lower temperature peak for SWCNT corresponds to the oxidation of carbon atoms while the concurrent thermal effect starting at 871.5 K represents the oxidation of the remaining Fe dopant.

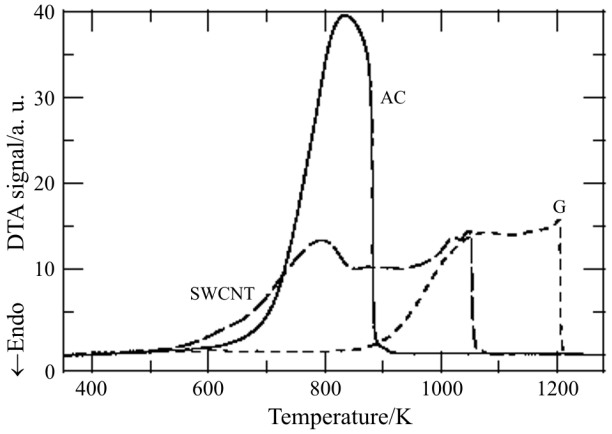

Fig. 1 DTA traces of the high-temperature oxidation of AC powder, SWCNT grain and G pellet samples in flowing dry air atmosphere at 10 K min^{-1}

The DSC signal from both AC (Fig. 2a) and SWCNT (Fig. 2b) samples in a flowing oxygen atmosphere and open sample pans shows an extensive exothermal effect practically throughout the whole instrumental temperature range having the transformation enthalpy ΔH_{AC}= –29,390 J g^{-1} and $\Delta H_{SWCNT}\geq$ –24,109 J g^{-1}. This exotherm evidently corresponds to more than one transformations. Thus, the main oxidation peak culminating consistently with DTA above $T_{x,AC}$=741.4 K and $T_{x,SWCNT}$=673.2 K (both for β= 10 K min^{-1}) is preceded by another broad exothermal peak. This effect is particularly well seen at higher heating rates (e.g. see the gray lines in Fig. 2a for AC). The main oxidation peak itself is affected by various controlling phenomena, too (such as the rate of heat

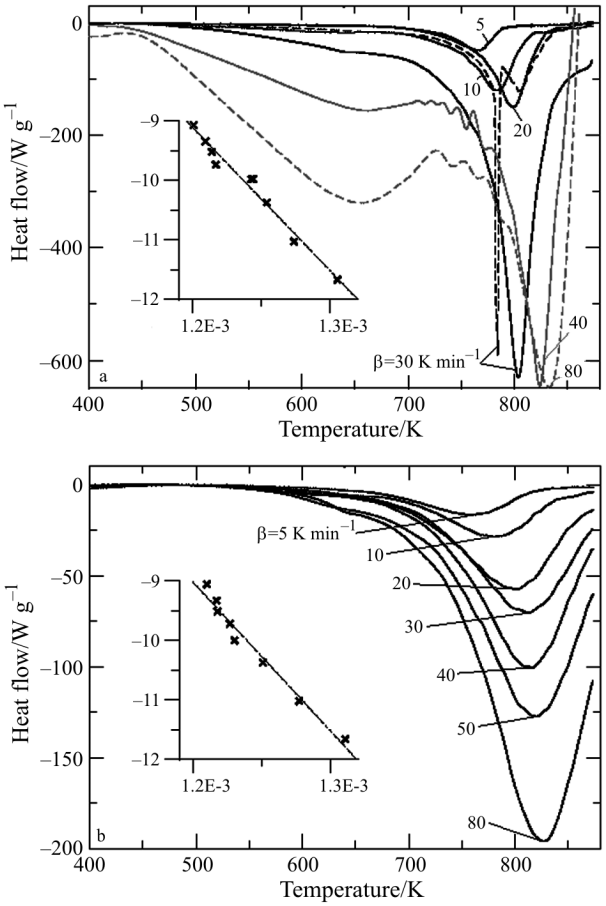

Fig. 2 Heating rate dependence of the DSC for the oxidation of a – AC and b – SWCNT in flowing oxygen atmosphere. In the insets, Kissinger plots, $\ln(\beta / T_p^2)$ *vs.* $1/T_p$

transfer or the rate of mass transfer), as will be discussed later in the interpretation. Assuming that only one rate controlling process is dominant at temperatures around the maximum of the main oxidation peak, $T_{p,AC}$ or $T_{p,SWCNT}$, the heating rate dependence of the peak might determine its activation enthalpy [3], $\Delta E^*_{K,AC}$ =200±12 kJ mol^{-1} for AC and $\Delta E^*_{K,SWCNT}$ = 208±14 kJ mol^{-1} for SWCNT, respectively. Due to the extremely small sample mass, the traces taken from AC at rates higher than 30 K min^{-1} (the gray lines) are plotted in artificially enlarged *y*-axis scales.

In TG heating the samples under the same experimental conditions to DSC, two opposite changes of their mass can be observed (Figs 3a and b). Firstly, starting already at the ambient temperature, the sample mass continuously increases up to 121 mass% for AC and 151% for SWCNT, probably indicating the chemisorption of oxygen atoms. It is in accordance with the other authors as in [4] for the case of graphite. At higher temperatures after the break point $T_{b,AC}$= 615.3 K or $T_{b,SWCNT}$=633.7 K, respectively (both for β=10 K min^{-1}), the sample mass dramatically vanishes

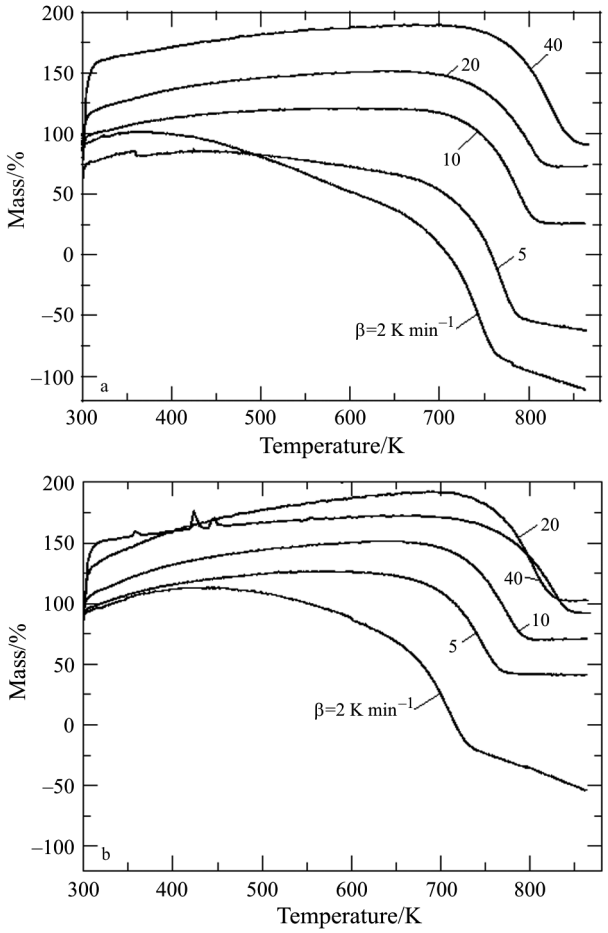

Fig. 3 Heating rate dependence of the TG for the oxidation of a – AC and b – SWCNT

(up to 100 mass% for AC and 80 mass% for SWCNT) following the kinetics of the formal chemical reaction $C+O_2 \rightarrow CO_2$. The shape of the DSC curves (as it was mentioned above) also indicates that the assumption of two transformations is probably correct.

Discussion

Specific peculiarities of the main oxidation peak were known by the series of DSC experiments, when the sample mass of AC was modified by more than one order. It may consist of two peaks for larger samples (>0.1 mg) and higher heating rates; the first peak is always very steep and sharp whereas the second peak is broad and smooth (see e.g. the dashed curve for β=30 K min^{-1} in Fig. 2a). This phenomenon was already observed when the chemical or physical processes in the sample were fast. Neeft *et al*. [5] theoretically analyzed that a limited heat transport in combination with large heat production may be at least partly responsible for such phenomenon in the case of the oxidation of soot. Thus in the first period, a thermal runaway occurs because the heat dissipation of the massive sample is slow compared with the heat that is generated by the reaction. The reaction rate then increases due to the overheating, so that the reaction generates more heat, which again accelerates the reaction, etc. Temperature in the center of the sample then becomes very high, and the reaction proceeds under oxygen mass-transfer limited conditions. When the sample in the center has burnt, its oxidation proceeds in the more outer regions and a gradual change in the process controlling the reaction occurs – from oxygen mass-transfer limitation to a temperature-controlled reaction rate. The conclusion must be that in the double-peak patterns both heat- and mass-transfer limitations occur. The mutual relation between these two rate limiting contributions, and thus the shape of the final curve, can be modified by variation of the sample mass and the external diffusivity of the reagent gas as it is seen in Fig. 4 for the variability in the sample mass of the order $4.5 \cdot 10^2$ and 100% change of the oxygen flow rate (also numerically in Fig. 6 in [5]). No thermal runaway effect has been observed in the case of SWCNT sample, a fact which is not surprising due to its 75 times higher heat transfer coefficient [6].

In our calculations we assume, similarly as other authors [7, 8] that the kinetics of the AC and SWCNT oxidation is controlled by the first order chemical reaction having the kinetic exponent, $0.5 \leq n \leq 1$ (the for-

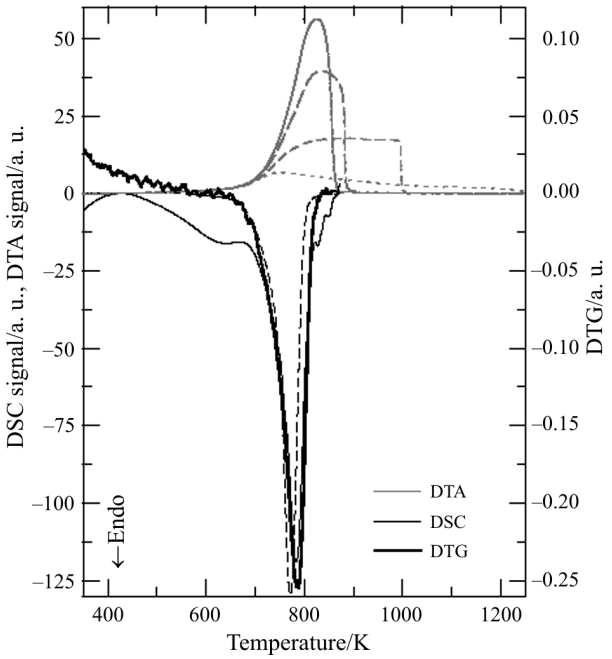

Fig. 4 Variability of the curves for the oxidation of AC depending on the experimental method (DTA, DSC, DTG) and the external diffusivity of the reagent gas; — – flowing oxygen or air atmosphere and open pans, --- – semi-closed and closed pans, ··· – static air atmosphere. Heating rate is 10 K min^{-1}

mal phase boundary reaction controlled kinetics when n=1, the reaction controlled by contracting volume when n=2/3 or by contracting area when n=1/2 [9]) and that the effect of diffusion can be neglected under the used experimental conditions

$$d\alpha/dt = kf(\alpha) = k(1-\alpha)^n$$

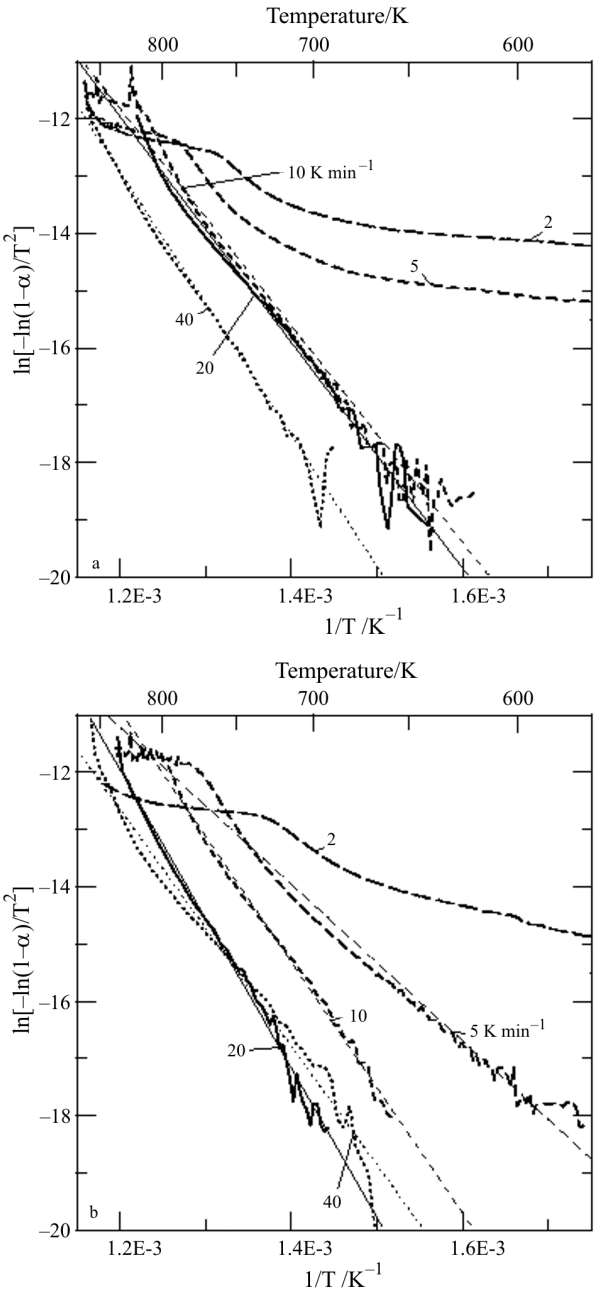

Fig. 5 Coats and Redfern plots from the TG curves (heating rate being the parameter) for the nonisothermal oxidation process of a – AC and b – SWCNT assuming first order kinetics. The slopes of the approximated straight-line dependencies (thin lines) give apparent activation energies $E^*_{CR,AC}$=176±2 kJ mol^{-1} and $\Delta E^*_{CR,SWCNT}$= 183±1 kJ mol^{-1} in the case of 10 K min^{-1}

where t is time, k is the temperature dependent Arrhenius rate constant, $k=A\exp(-\Delta E^*/RT)$. R is the gas constant, the model parameters A and E^* are the frequency factor and activation enthalpy. The degree of conversion α, (fraction of sample reacted) is given by the expression $\alpha(t)=(m_i-m_t)/(m_i-m_f)$, where m_i and m_f are the initial and final percent masses and m_t the percent mass at time t as they are collected from a TG experiment. (The real time and temperature are simply related through the constant heating rate, $T=T_0+\beta t$, in each TA technique.) The parts of the TG curves corresponding to the range of conversion $a\in(0.05–0.95)$ were taken for calculations. The differential Kissinger method resulting in the activation enthalpy, ΔE^*_K [3] and the integral Coats and Redfern method (assuming n=1 or 2/3) resulting in the activation enthalpy, ΔE^*_{CR} [10], were used for comparative calculations. In both cases, the calculated activation enthalpy corresponds to the best linear dependence calculated applying the least squares method. Namely, the discrete temperature of the maximal reaction rate, T_p, was found for each heating rate, β, from all DTG curves (DTG is the time derivative of TG) and $\ln(\beta/T_p^2)$ *vs*. $1/T_p$ deduced $\Delta E^*_{K,AC}$ =201±8 kJ mol^{-1} for AC and $\Delta E^*_{K,SWCNT}$ =119±5 kJ mol^{-1} for SWCNT in the case of Kissinger. $\ln[g(\alpha)/T^2]$ *vs*. $1/T$ was applied in the case of Coats and Redfern (CR) for any complete continuous heating curve where $g(\alpha)=\int d\alpha/f(\alpha)$. If n=1, the CR plots show parallel straight lines deducing $\Delta E^*_{CR,AC}$ =176±2 kJ mol^{-1} for β≥10 K min^{-1} in the case of AC (Fig. 5a) and $\Delta E^*_{CR,SWCNT}$ = 183±1 kJ mol^{-1} in the case of SWCNT (Fig. 5b). Besides, the participation of another microprocess is particularly seen in the initial stages of the main transformation at slower heating rates. Assuming that n=2/3, the CR curve fitting procedure would reveal the more pronounced heating rate dependence of both kinetic parameters (at the same coefficient of determi-

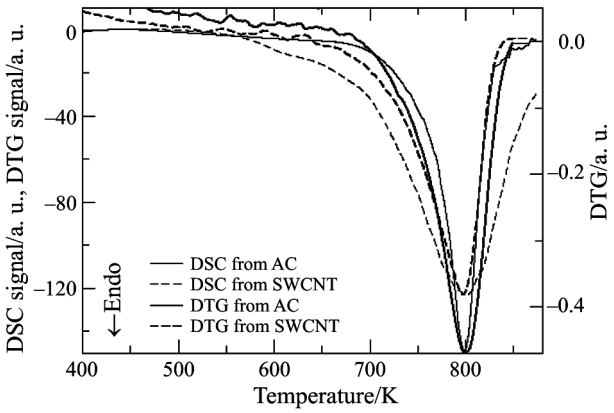

Fig. 6 Relation between the DTG and DSC oxidation peaks from AC and SWCNT at 20 K min^{-1}. DSC curves are scaled to the DTG curves

nation r^2=0.95) and systematically lower activation enthalpies, namely $\Delta E^*_{CR,n=2/3} \sim 0.93\Delta E^*_{CR,n=1}$ for AC and $\Delta E^*_{CR,n=2/3} \sim 0.89\Delta E^*_{CR,n=1}$ for SWCNT in the case of β=10 K min^{-1} (as it was already observed for graphite [7, 11]).

Both Kissinger and Coats and Redfern fits revealed the good linearity however different activation enthalpies were achieved. Moreover, ΔE^*_{CR} was disvaluated due to its significant dependence on *n*. In [12], the kinetics of very pure crystalline cellulose was investigated in isothermal and dynamic mode. Complicated profile of TG and DTG curves has been demonstrated. The authors tested all common kinetic models and applied various mathematical treatments. They evidenced that the Kissinger parameter of the main reaction, ΔE^*_K, being 200 kJ mol^{-1} varies by only 1.3% from the optimized value calculated by the most satisfactory reaction scheme and the non-linear numerical curve fitting procedure in this case. The 'Kissinger simplification' might be accepted in our case, too, before the complex kinetic analysis including the isothermal data will not be available.

Slanina *et al*. reported a computational study of room temperature oxygen additions to narrow nanotubes (with the diameter of 4 or 5 Å consisting of 84 or 80 atoms) [13]. Though there is no argument for any parallel between these theoretical predictions and our experimental observations (our SWCNT is a mixture of all types of nanotubes with a mean diameter of 15 Å), at least both thermodynamic and kinetic quantitative similarities of the results seem to be interesting. So, our $\Delta H_{exp} \geq 24.11$ kJ g^{-1} and ΔE^*_{exp} =119 kJ mol^{-1} values (being to total heat of both transformation steps and the activation enthalpy of the main process) are comparable with the computed heat of formation and activation enthalpy for breaking of one of two possibly most frequently occurring C–C bonds (namely ΔH_t=17.9 kJ g^{-1} and ΔE^*_t =120.5 kJ mol^{-1} for the bond 1–17) in the case of the I_hC_{20} model nanotube, (Table 1 in [13]).

From the thermodynamic standpoint (the parallel between our measured and theoretically predicted [13] heats of transformation), both carbon forms undergo complex chemical transformations (probably firstly the chemisorption of oxygen atoms, later chemical reaction could be hypothesized). From the other point of view, the mutual relation between various elementary reaction steps in the course of the complex high-temperature oxidation of any carbon form has not yet been resolved. In Fig. 6, the coincidence between the DSC and DTG kinetics is illustrated for the oxidation reaction in AC and SWCNT. Exhibiting similar shape and maximums at the same temperatures (for β=20 K min^{-1}) the DSC peak is slightly narrower for AC while it is significantly wider for SWCNT than the DTG ones. Therefore, we conclude that DSC and DTG data need not represent the same rate controlling processes in the carbonaceous samples. So, only apparent kinetic parameters could be deduced. Due to complex heat- and mass-transfer limitations in AC and SWCNT samples, different complex ΔE^*_K have been determined by DSC (scanning the heat) and DTG (inspecting the mass and resulting in similar absolute values as in [7, 11]) methods. The difference in the ratio of $\Delta E^*_{K,DSC} / \Delta E^*_{K,DTG}$ for AC and SWCNT reflects the various proportionality of the two transfer limitations. Moreover, ΔE^*_K, since deduced by the DSC experiment under the condition of varying sample mass, might have a lower methodological credibility.

Conclusions

AC is highly reactive and structurally less ordered form of carbon. On the contrary, SWCNT possessing a high structural ordering should be more oxidation resistant. Our results have shown that in general the high-temperature oxidation reaction in AC and SWCNT is similar.

Both DSC and TG indicated two mutually overlapping transformation steps, namely first the thermally activated chemisorption of oxygen atoms above the room temperature and later the degradation of each sample mass by a massive reaction above ~600 K, in the course of heating the AC and SWCNT samples.

The kinetics of the main oxidation effect is both heat- and mass-transfer limited in all carbon forms. The mutual relation between these two rate limiting contributions depends not only on the topological micro-ordering (AC or SWCNT) and macro-ordering (morphology of the sample surface), however, on the sample mass, as well.

Due to the complex character of the thermal oxidation of carbon, each individual phenomenological method for the thermal analysis can give only the apparent kinetic parameters (*n*, Δ*E**) reflecting the actual proportionality of the rate controlling processes.

Acknowledgements

This work was supported by the Grants VEGA 2/5096/25, 2/1127/23 and APVT-51052702 and by the SAS Center of Excellence 'Nanosmart'. Solid State Research group from the Max Planck Institute in Stuttgart is acknowledged for the samples.

References

1 E. Hennberg, B. Bernhardt and K. Bohmhammel, Thermochim. Acta, 415 (2004) 43.
2 E. Illeková, V. Skákalová, J. Čech, U. Dettlaff and S. Roth, DSC study of the sorption ability of various forms of carbon, 305. WE-Heraus-Seminar: Carbon Nanotubes, 2–5 November, 2003, Bad Honnef, Germany.
3 H. E. Kissinger, Annal. Chem., 29 (1957) 1702.
4 R. Schlogl, G. Loose and M. Wasemann, Solid State Ionics, 43 (1990) 183.
5 J. P. A. Neeft, F. Hoornaert, M. Makkee and J. A. Moulijn, Thermochim. Acta, 287 (1996) 261.
6 V. Vretenár, V. Skákalová and S. Roth, Thermal conductivity of single wall carbon nanotubes, 305. WE-Heraus-Seminar: Carbon Nanotubes, 2–5 November, 2003, Bad Honnef, Germany.
7 S. Valová, V. Slovák and J. Leško, Acta Metall. Slovaca, 6 (2000) 304.
8 S. Gajewski, H.-E. Maneck, U. Knoll, D. Neubert, I. Dörfel, R. Mach, B. Strauß and J. F. Friedrich, Diamond Relat. Mater., 12 (2003) 816.
9 J. Šesták, Thermophysical properties of solids, Academia Prague, 1984, p. 419.
10 A. W. Coats and J. P. Redfern, Nature, 201 (1964) 48.
11 V. Slovák, Thermochim. Acta, 372 (2001) 175.
12 Z. Slanina, L. Stobinski, P. Tomasik, H.-M. Lin and L. Adamowicz, J. Nanosci. Nanotech., 3 (2003) 193.
13 R. Capart, L. Khezami and A. K. Burnham, Thermochim. Acta, 417 (2004) 79.